

# The stability and degradation of PECVD fluoropolymer nanofilms

James Bowen<sup>1</sup>, David Cheneler<sup>2\*</sup>

<sup>1</sup> School of Engineering and Innovation, The Open University, Walton Hall, Milton Keynes, MK7 6AA, UK

<sup>2</sup> Engineering Department, Lancaster University, Bailrigg, Lancaster, LA1 4YR, UK

\* Corresponding author: d.cheneler@lancaster.ac.uk

## Abstract

Fluoropolymer films are frequently used in microfabrication and for producing hydrophobic and low-k dielectric layers in various applications. As the reliability of functional coatings is becoming a more pressing issue in industry, it is necessary to determine the physical stability and degradation properties of this important class of films. To this end, a study has been undertaken to ascertain the aging characteristics of fluoropolymer films under various environmental conditions that such a film may experience during its use. In particular, fluorocarbon films formed by plasma-enhanced chemical vapour deposition (PECVD) using octafluorocyclobutane, or  $c\text{-C}_4\text{F}_8$ , as a precursor gas have been exposed to abrasive wear, elevated temperatures, ultraviolet radiation, as well as oxygen plasma and  $\text{SF}_6$  plasma, the latter being commonly used in conjunction with these films in ion etching processes. The results show that sub-micron thick fluoropolymer films exhibit a significant amount of elastic recovery during nanoscratch tests, minimising the impact of wear. The films exhibit stability when exposed to 365 nm UV light in air, but not 254 nm light in air, which generated significant decreases in thickness. Exposure to temperatures up to 175 °C did not generate loss of material, whereas temperatures higher than 175 °C did. Etching rates upon exposure to oxygen and  $\text{SF}_6$  plasmas were also measured.

## Keywords

Octafluorocyclobutane, plasma deposition, atomic force microscopy, wear, ellipsometry

## 1. Introduction

Fluorocarbon gases such as  $\text{CF}_4$ ,  $\text{C}_2\text{F}_6$  and  $\text{C}_4\text{F}_8$  have been used in microfabrication industries for over twenty years [1]. They are used for several purposes, especially the selective etching of Si and  $\text{SiO}_2$  [2-3] and high aspect ratio structures through the Bosch process [4-6], and depositing intermetallic low-k dielectric films [7-9]. Fluoropolymer films are used as interlayer dielectrics because the C-F bonds have a much weaker tendency to polarise in external electric fields as compared to O-H and C-H bonds found in other common films [7]. These bonds also act to reduce a surfaces van der Waals interaction with water making fluoropolymer films both hydrophobic as well as lipophobic [10]. These properties combined with these films characteristic conformal coating and adhesion properties [11] means as a result, fluoropolymer films have found application in other important areas. These areas include industrially and commercially relevant commodities such as superhydrophobic glasses and windscreens [12] and microfluidic devices with controlled wetting and valving [13-14] as well as nanocoated/patterned surfaces for more fundamental studies such as cell research [15-16].

A common method of deposition for these films is plasma-enhanced chemical vapour deposition (PECVD) [7]. This is because, primarily, the technique is compatible with standard microfabrication techniques, but more generally, because organic precursor materials, usually in gaseous form, are commonly used as initial materials for the polymerisation process. If the more common thermal CVD methods were used, the temperatures are frequently much higher than in PECVD, potentially damaging the organic precursors and formed oligomers and preventing polymerisation on the substrate surface. In contrast, during PECVD, the precursor materials are decomposed into various components (atoms and molecules in ground and excited states, ions, electrons and free radicals) through collisions with highly accelerated charged particles, i.e. the electrons and ions. The highly reactive components deposit on the relatively cold substrate in a heterogeneous chemical reaction, forming a polymerised film.

Cyclic octafluorocyclobutane or  $c\text{-C}_4\text{F}_8$ , is a popular precursor gas for the deposition of fluoropolymer films [17-19], and is the material that will be focussed upon here.  $c\text{-C}_4\text{F}_8$  has a highly strained ring structure composed of  $\text{-CF}_2\text{-}$  units [20]. This ring is readily opened by electron impact [18-19], most probably through the following decomposition branch:



This is consistent with data available for thermal and multiphoton dissociation [18], although it should be noted that other minor branchings are possible through electron impact dissociation to form  $\text{CF}$ ,  $\text{CF}_2$ ,  $\text{CF}_3$  and  $\text{C}_3\text{F}_5$ . Since  $\text{CF}_2$  is the most likely product in  $\text{C}_2\text{F}_4$  thermal dissociation reactions, the most likely electron impact dissociation of  $\text{C}_2\text{F}_4$  is [18]:



Other dissociation branchings are possible as are other reactions such as ion-neutral particle reactions, electron-ion reactions and neutral heavy particle reactions. This latter reaction, whilst not very important at the pressures commonly used in PECVD ( $< 10$  mTorr) can drive gas-phase reactions to form gas-phase oligomeric species, not necessarily formed from the direct decomposition of the precursor gases [21]:



It is thought that these oligomeric units, in conjunction with  $\text{CF}_2$ , contribute to the surface passivation and film growth [21].

In order to facilitate plasma reactor design and process optimisation, over the years there have been numerous studies on the behaviour of fluoropolymer films, including those formed from  $c\text{-C}_4\text{F}_8$  precursor gas [17-23]. Therefore, the chemical and physical composition of fluoropolymer films are pretty well known. As is the chemical stability of these films [24, 25]. However, less is known about their mechanical stability and degradation characteristics. This is increasing relevant as this one aspect can limit the uptake of fluoropolymer films in new products and processes as a functional coating. It is known that fluoropolymer films fare reasonably well during chemical/mechanical planarization (CMP) processes undertaken during wafer fabrication [7], and that they increase scratch resistance by reducing the friction when used as an additive to other polymer films [26], and hence show a great deal of potential. Therefore, the mechanical stability and degradation characteristics of fluoropolymer films is worthy of further study.

As well as all the other potential decomposition branchings and possible reactions that can occur during the PECVD of fluoropolymer films, the substrate can have an effect. In this paper, we study the physical stability and degradation of fluoropolymer films on a silicon substrate as commonly used in the microfabrication industry. As noted earlier, fluorocarbon gases, such as that formed in the decomposition of the precursor gas  $c\text{-C}_4\text{F}_8$ , can etch the native  $\text{SiO}_2$  surface. This means that oxygen may be present in the films (it may also be present as a common additive, or as residual gas in an imperfect vacuum) so that they are more accurately defined as  $\text{CF}_x\text{O}_y$  thin films.

In this paper,  $\text{CF}_x\text{O}_y$  thin films are exposed to abrasive wear, elevated temperatures, ultraviolet radiation, as well as oxygen plasma and  $\text{SF}_6$  plasma. The aim of the work is to determine those conditions which lead to a degradation and removal of  $\text{CF}_x\text{O}_y$  films when exposed to such conditions. To the best of our knowledge, such information does not currently exist in the published literature. It is anticipated that the results presented here will be of practical significance to microelectromechanical systems engineers, including those researchers who work with fluoropolymer thin films and desire data to inform projected product performance and life expectancy.

## 2. Experimental

### 2.1 Deposition of plasma-polymerised $CF_xO_y$ films

Plasma-polymerised  $CF_xO_y$  films were deposited onto the polished side of single crystal N-type Si (100) wafers (Si-Mat, Germany) using a STS Multiplex ICP DRIE etcher (STS Plc., UK), utilising  $C_4F_8$  gas (Pelchem, South Africa). The gas flow rate was 85 sccm (standard cubic centimetres per minute) at a pressure of 36 mTorr. The coil power was 300 W and the platen power was 110 W. Wafers were used as received, with any visible dust or debris being removed by sweeping the surface with  $N_2$  gas. All sample handling was carried out using tweezers (Agar Scientific, UK) to minimise the risk of sample contamination. Films of nominal thickness of 210 nm, 328 nm and 558 nm were deposited by varying the deposition time. Film thickness, as measured by ellipsometry, varied by no more than  $\pm 1$  nm across the central region of the wafer from which samples were taken.

### 2.2 Film thickness

Film thicknesses were measured using a UVISEL ellipsometer (Horiba Jobin-Yvon, UK) over the wavelength range 250-800 nm and at an angle of incidence of  $70^\circ$ . All measurements were made under ambient conditions ( $19^\circ C$ ,  $<35\%$  RH) and precautions were taken to avoid performing measurements on visibly defective sample locations. Calculation of the  $CF_xO_y$  film thickness was performed for each measurement, based on a four-phase ambient/ $CF_xO_y$  film/ $SiO_2$ /Si model, in which the  $CF_xO_y$  film was assumed to be isotropic and modelled as a Classical Lorentzian oscillator. Film thicknesses are presented as mean values accurate to  $\pm 1$  nm, based on a minimum of three non-overlapping measurements.

### 2.3 Film topography

Images were acquired using a NanoWizard II AFM (JPK Instruments, UK) operating in Contact Mode at a temperature of  $18^\circ C$  and a relative humidity of  $<40\%$ . Rectangular pyramidal-tipped Si cantilevers (CSC17/noAl, MikroMasch, Estonia) with a nominal tip diameter of  $<10$  nm were employed. Samples analysed using the AFM were held in place using a custom-built magnetic sample stage. Two-dimensional image analysis was performed using Scanning Probe Image Processor software (Image Metrology, Denmark); plane correction was performed using linewise levelling. Average roughnesses are presented as mean values, based on a minimum of three non-overlapping measurements. The variation in average roughness between each measurement performed was  $<5\%$ .

### 2.4 Assessment of film composition by X-ray photoelectron spectroscopy

XPS analysis was performed using an Escalab 250 system (Thermo VG Scientific, UK) operating with Avantage v1.85 software. An Al  $K\alpha$  X-ray source was used, providing a monochromatic X-ray beam with incident energy of 1486.68 eV. The measurements were made at a pressure of  $\sim 5 \times 10^{-9}$  mbar and with a circular spot size of  $\sim 0.2$  mm<sup>2</sup>. Samples were immobilised onto stainless steel sample holders using double-sided carbon sticky tape (Shintron tape, Shinto Paint Company, UK). Low-resolution survey spectra were obtained using a pass energy of 150 eV over a binding energy range of -10 to 1,200 eV with 1 eV increments. Low-resolution spectra would typically be obtained from an average of 5 scans. High-resolution spectra were obtained using a pass energy of 20 eV over a binding energy range of 20-30 eV, centred around a chosen photoelectron binding energy with 0.1 eV increments. A dwell time of 20 ms was employed when collecting data from each binding energy increment for all measurements. High-resolution spectra would typically be derived from an average of at least 10 scans.

### 2.4 Abrasive wear tests using AFM

Abrasive wear tests were performed using a NanoWizard II AFM (JPK, UK) operating in contact mode using rectangular pyramidal-tipped Si cantilevers (PPP-NCL, Windsor Scientific, UK) with a nominal tip diameter of 20 nm. Wear tests were performed over an area of  $1 \times 1$   $\mu m$  at a tip velocity of  $4 \mu m s^{-1}$  under conditions of (i)  $19^\circ C$ ,  $<35\%$  RH; and (ii)  $100^\circ C$ ,  $<35\%$  RH. Compressive normal loads in the range 0.5-3  $\mu N$  were employed.

### 2.5 Exposure to elevated temperatures in air

$CF_xO_y$  films of nominal thickness 558 nm were exposed to elevated temperatures in air. Samples were mounted on a High Temperature Heated Stage (HTHS, JPK Instruments, UK) for the following treatments: (i)  $100^\circ C$  for 21 h; (ii) 200

°C for 18 h; (iii) 200 °C for 63 h. Further, the HTHS was mounted on the UVISEL ellipsometer, following which a heating/cooling cycle was performed in step-wise fashion between 25-200 °C, measuring the film thickness at 25 °C intervals. All temperatures were maintained using the closed-loop control system of the HTHS, which meant that temperatures varied by no more than  $\pm 1$  °C during a 'temperature hold' period.

### *2.6 Exposure to ultraviolet (UV) radiation*

CF<sub>x</sub>O<sub>y</sub> films of nominal thickness 558 nm were housed in a bespoke environmental chamber (Longshore Engineering, UK) and exposed to ultraviolet (UV) light for 21 h. This was achieved using a UVLS-28 EL Series UV Handheld Lamp (Analytik-Jena, USA). The atmosphere around the sample was either (i) ambient air, or (ii) nitrogen gas. UV light of wavelengths 254 nm and 365 nm were used. The chamber consisted of CaF<sub>2</sub> windows, permitting efficient transmission of the UV light.

### *2.7 Exposure to oxygen plasma and SF<sub>6</sub> plasma*

CF<sub>x</sub>O<sub>y</sub> films of nominal thickness 558 nm were exposed to oxygen plasma and sulphur hexafluoride (SF<sub>6</sub>) plasma. Films were exposed to both plasmas using a STS Multiplex ICP DRIE etcher (STS Plc., UK), utilising O<sub>2</sub> and SF<sub>6</sub> gas (BOC, UK) respectively. In both cases, the flow rate of the gas was 50 sccm with a pressure of 5 mTorr. The platen power was set to 100 W and the RF coil power to 600 W.

### 3. Results and Discussion

#### 3.1 Abrasive wear tests using AFM

Figures 1-2 show the results of the abrasive wear tests performed using AFM. This nanoscale scratch test emulates the effect of contact with nano-asperities. Figure 1 presents line profiles extracted from AFM images recorded of the worn surface, for each combination of film thickness, temperature, and normal load tested. Line profiles are presented in order of increasing normal load,  $W = 0.5 - 3.0 \mu\text{N}$ , vertically downwards in each image. Contact pressures were calculated to be in the range 3.6 – 6.6 GPa, assuming an AFM tip radius of 10 nm and a Young's modulus of 7 GPa [24] for the  $\text{CF}_x\text{O}_y$  film. Figure 2 shows the maximum penetration depths generated from the abrasive wear tests.

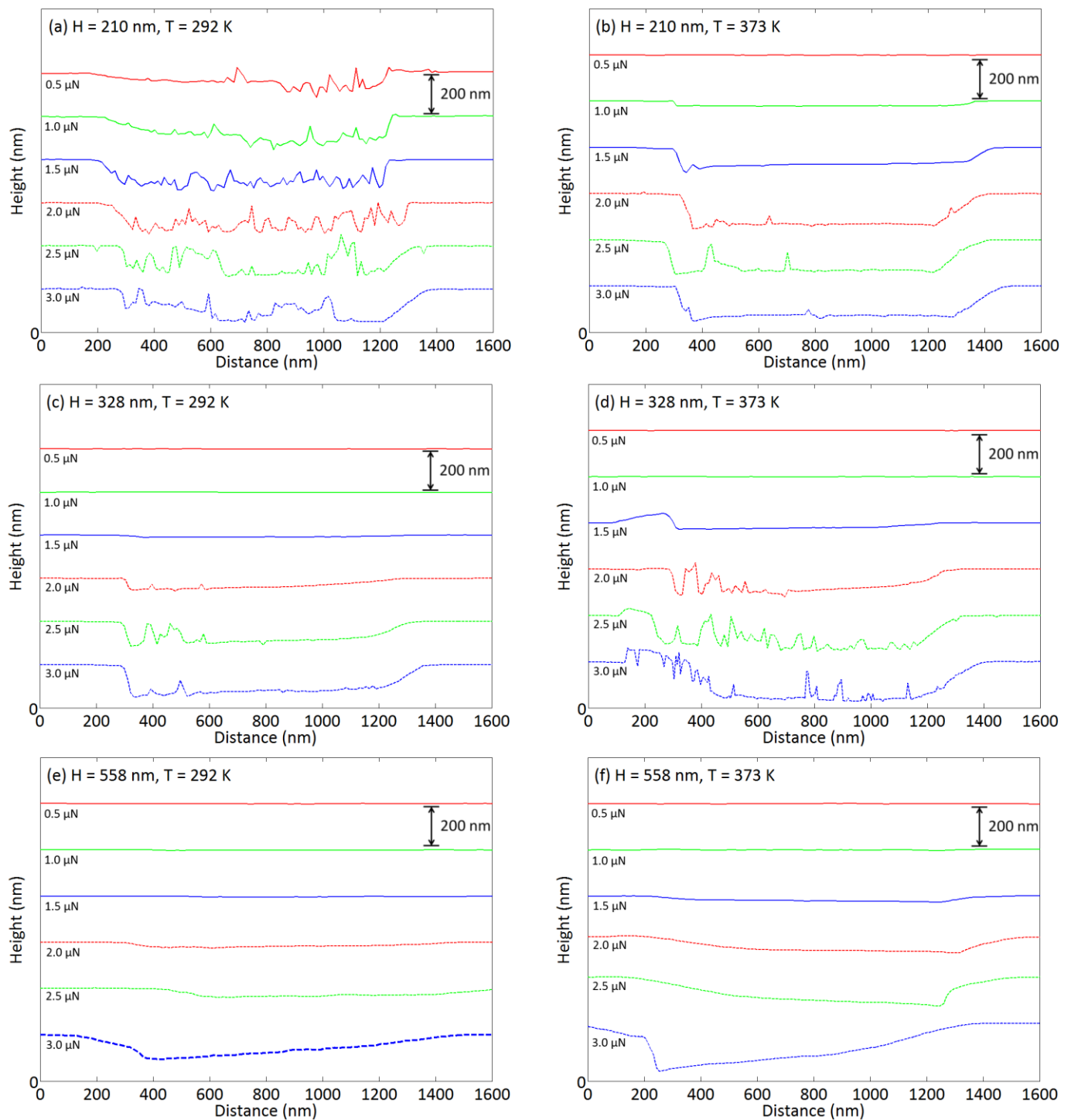


Figure 1. Line profiles obtained by atomic force microscopy for  $\text{CF}_x\text{O}_y$  films of thickness  $H$  exposed to abrasive wear at temperature  $T$ : (a)  $H = 210 \text{ nm}$ ,  $T = 292 \text{ K}$ ; (b)  $H = 210 \text{ nm}$ ,  $T = 373 \text{ K}$ ; (c)  $H = 328 \text{ nm}$ ,  $T = 292 \text{ K}$ ; (d)  $H = 328 \text{ nm}$ ,  $T =$

373 K; (e)  $H = 558$  nm,  $T = 292$  K; (f)  $H = 558$  nm,  $T = 373$  K; line profiles are presented in order of increasing normal load,  $W = 0.5 - 3.0$   $\mu\text{N}$ , vertically downwards in each image.

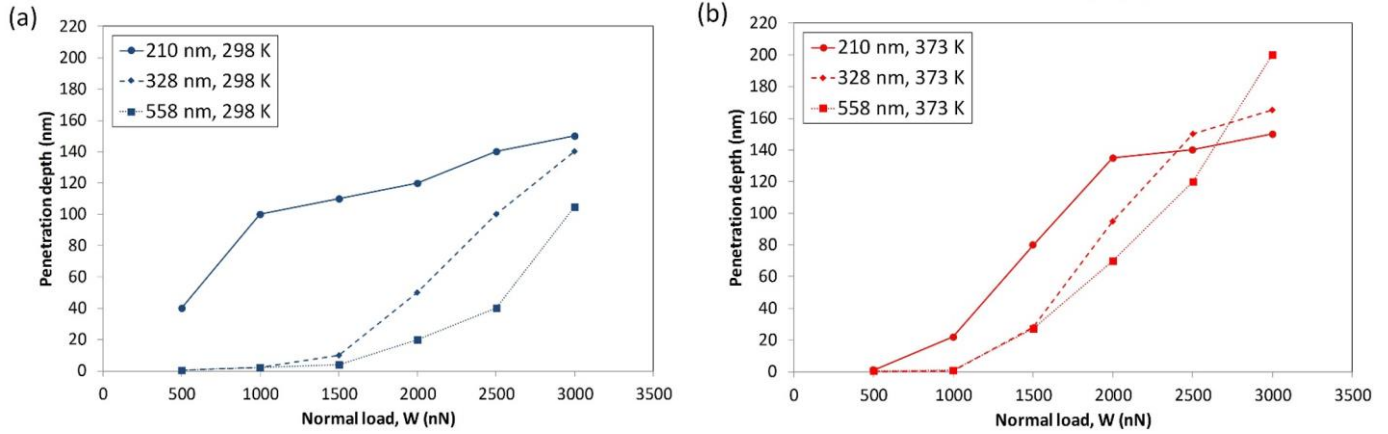


Figure 2. Maximum penetration depths generated from the abrasive wear tests.

Figure 1 reveals that the wear tests performed at 292 K generated rougher surfaces than those performed at 373 K. Figure 2 shows that the maximum penetration depth depends strongly on film thickness and normal load at 292 K, yet does not depend significantly on film thickness at 373 K. Dimensionless wear coefficients,  $k$ , are in the range  $10^{-3} < k < 5 \times 10^{-2}$ . Wear coefficients at 292 K were similar to wear coefficients at 373 K for normal loads  $W > 1,500$  nN, whereas for  $W < 1,500$  nN the wear coefficients were lower for 373 K than for 292 K. The Archard equation was used to calculate the wear coefficient, and is given by:

$$k = \frac{VH}{WL} \quad (1)$$

where  $V$  is the volume of material displaced,  $H$  is the film hardness,  $W$  is the normal load, and  $L$  is the distance travelled. The hardness was calculated using equation 2, where the film stiffness,  $s$ , was obtained from the indentation region of AFM load-displacement data acquired during the wear tests ( $s \sim 30$  N m<sup>-1</sup>).

$$H = \frac{s}{2\pi R} \quad (2)$$

where  $R$  is the radius of curvature of the AFM cantilever tip ( $R = 10$  nm).

The percentage composition of the  $\text{CF}_x\text{O}_y$  films as determined by XPS was found to be approximately 50 % carbon and 50 % fluorine, with a small amount of oxygen, generally less than 2 %, occasionally detected. While the  $\text{C}_4\text{F}_8$  monomer has a 2:1 mole ratio of fluorine to carbon, it is understood that some fluorine is lost as a gas during the plasma polymerisation. The principal peaks in the C 1s photoelectron spectra for all  $\text{CF}_x\text{O}_y$  films are attributed to the photoelectrons from the C-F and C-F<sub>2</sub> bonds in the films. The remainder of the spectra consists of photoelectrons from the C-F<sub>3</sub>, C-C-F and C-C bonds. Slight O 1s photoelectron peaks were observed for all  $\text{CF}_x\text{O}_y$  films, while no Si 2p photoelectron peaks were observed. This suggests that C 1s photoelectrons from C-O-C and C=O bonds may also contribute to the C 1s photoelectron spectra. The carbon atoms in the film are expected to exhibit sp<sup>3</sup> hybridisation, with the exception of those present in C=O bonds, which will exhibit sp<sup>2</sup> hybridisation. It is expected the films will exhibit a high degree of cross-linking, which gives these films their high modulus. This also leads to very smooth films [27] covered with fluorine atoms, thus exhibiting low adhesion and friction [7].

This low friction reduces the tensile stress surrounding the sharp tip, and in turn the yield zone, and should therefore reduce the amount of plastic flow damage [28]. This plastic damage can manifest as groove formation and ploughing effects where material is pushed to the side of the scratch [25]. The significant roughness of the residual films in figures 1a and 1b where the troughs are comparable to the film thickness, suggests that ploughing has occurred, but that this may be adhesive failure rather than cohesive failure and that the scratches have gone through the whole film. As the films get thicker, the damage at low loads is minimal. This suggests a significant amount of elastic recovery upon removal of the applied scratch stress. The significant amount of residual damage in the thinnest film,

suggests that the stress is enhanced by the close proximity of the underlying substrate, which is consistent with thin-film indentation theory [29]. The relatively smooth profile of the deformed films at higher loads suggest plastic grooving is the primary mechanism for wear. The film surface, shown in Figure 3, suggests a 'sponge-like morphology', in-keeping with measurements performed elsewhere [19]. These surface structures may have collapsed under compression, leading to the permanent deformation shown in figures 1 and 2. However, given the degree of permanent deformation (10s-100s of nm) as compared to the surface morphology (< 10 nm), and that there is no evidence that the bulk of the film exhibits a porous nanostructure, this is unlikely, but this requires further investigation.

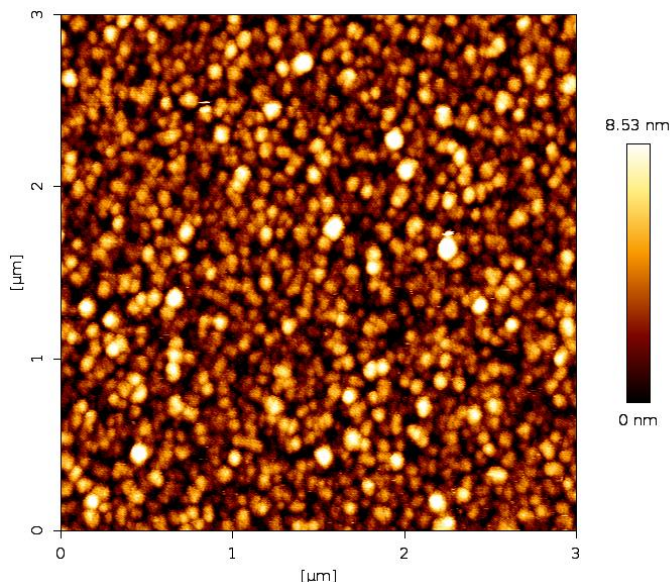


Figure 3.  $\text{CF}_x\text{O}_y$  film surface topography as measured using atomic force microscopy.

### 3.2 Exposure to elevated temperatures in air

Figure 4 shows the effect of elevated temperatures on the  $\text{CF}_x\text{O}_y$  film, demonstrating the increase and decrease in film thickness, measured using ellipsometry. The temperature was increased in step-wise fashion between 298-473 K. The film thickness increases with increasing temperature, exhibiting a coefficient of thermal expansion,  $\alpha \sim 1.02 \text{ K}^{-1}$ . Degradation begins on the heating cycle between 448 and 473 K, and continues on the cooling cycle as the temperature is decreased. For temperatures  $T < 390 \text{ K}$  the gradient of the Thickness/Temperature plots for the heating and cooling cycles are similar, suggesting that the changes in film thickness here are only due to thermal expansion and contraction.

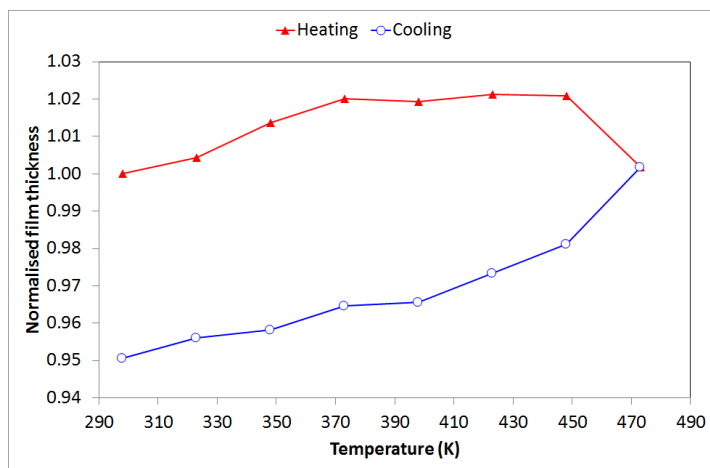


Figure 4. Effect of temperature on  $\text{CF}_x\text{O}_y$  film thickness.

Figure 5(a) shows that exposure to a temperature of 473 K in air caused a larger decrease in film thickness, 114 nm in 18 h, than exposure to a temperature of 373 K in air, 6 nm in 21 h. Exposure to 473 K for 63 h led to a film thickness decrease of 162 nm, demonstrating that the degradation occurs in a non-linear fashion. The change in thickness may be due to an evaporation of residual humidity from the surface. Alternatively, it may be because C–F bonds are thermally less stable than  $\text{CF}_2$  and  $\text{CF}_3$  bonding environment [7]. When the C–F bond breaks at elevated temperatures and fluorine disappears from the molecule,  $\text{CF}_3$  fragments can bond to the carbon. This may result in a densification of the film and a corresponding reduction in thickness. It has been suggested that an amorphous C–C cross-linked structure is necessary to increase the thermal stability [7].

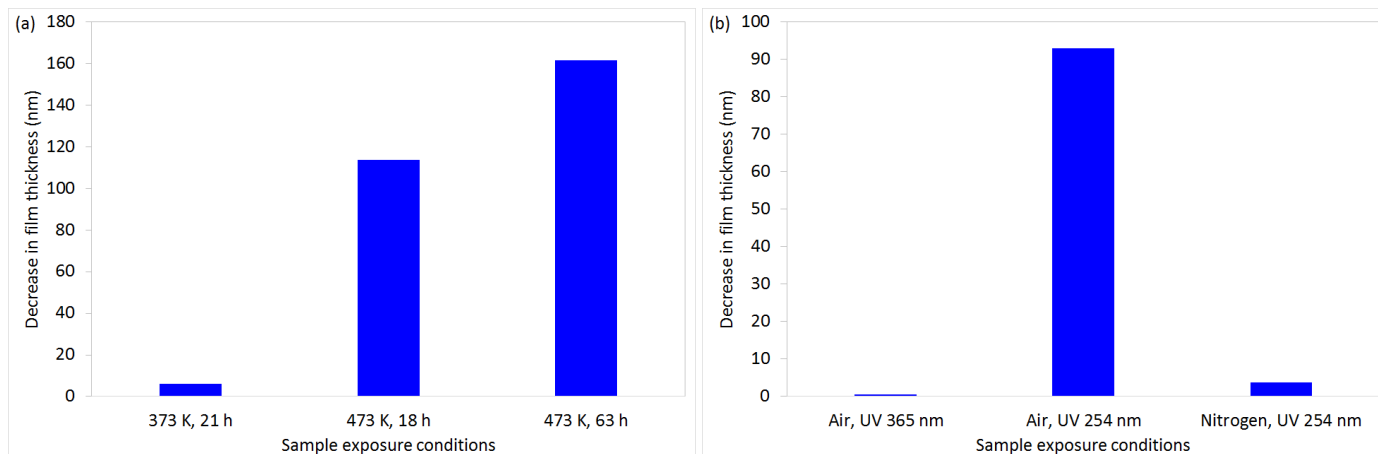


Figure 5. Decrease in  $\text{CF}_x\text{O}_y$  film thickness due to (a) exposure to elevated temperatures in air, (b) exposure to UV light for 21 h.

### 3.3 Exposure to ultraviolet (UV) radiation

Figure 5(b) shows that the  $\text{CF}_x\text{O}_y$  film degrades upon exposure to 254 nm UV light in the presence of air, but is almost undamaged by exposure to 365 nm UV light in the presence of air. UV light of wavelength 254 nm has an equivalent energy of  $471 \text{ kJ mol}^{-1}$ , which is sufficient to break C–C bonds ( $348 \text{ kJ mol}^{-1}$ ) and C–O bonds ( $360 \text{ kJ mol}^{-1}$ ) in the  $\text{CF}_x\text{O}_y$  film. C–F bonds ( $488 \text{ kJ mol}^{-1}$ ) are unlikely to be broken by 254 nm UV light. In comparison, 365 nm UV light has an equivalent energy of  $328 \text{ kJ mol}^{-1}$ , which is insufficient to break any of these chemical bonds. It is therefore suggested that film degradation occurs due to the generation of carbon and oxygen free radicals by the 254 nm UV light. Diffusion of these species away from the film prevents re-polymerisation from taking place, leading to mass loss and a decrease in film thickness.

### 3.4 Exposure to oxygen plasma and $\text{SF}_6$ plasma

Figure 6(a) shows that the  $\text{CF}_x\text{O}_y$  film is etched by both oxygen plasma and  $\text{SF}_6$  plasma, the latter being commonly used in conjunction with  $\text{C}_4\text{F}_8$  during DRIE processes. The rate of material removal is greater for the oxygen plasma (approximately  $11 \text{ nm s}^{-1}$ ) than for the  $\text{SF}_6$  plasma (approximately  $7 \text{ nm s}^{-1}$ ). The increased etch rate for the oxygen plasma is hypothesised to be due to reactive effects, whereas the  $\text{SF}_6$  plasma is thought to remove material only due to physical bombardment and mechanical attrition [25]. The  $\text{SF}_6$  plasma carries away  $\text{CF}_x$  fragments through dissociative attachment to the  $\text{SF}_6^-$  ions. Figure 6(b) shows that the surface roughness of the  $\text{CF}_x\text{O}_y$  film is decreased by the action of the  $\text{SF}_6$  plasma, whereas it remains approximately constant due to the action of the oxygen plasma. This result supports the hypothesis that the removal mechanisms are different for the two plasmas.

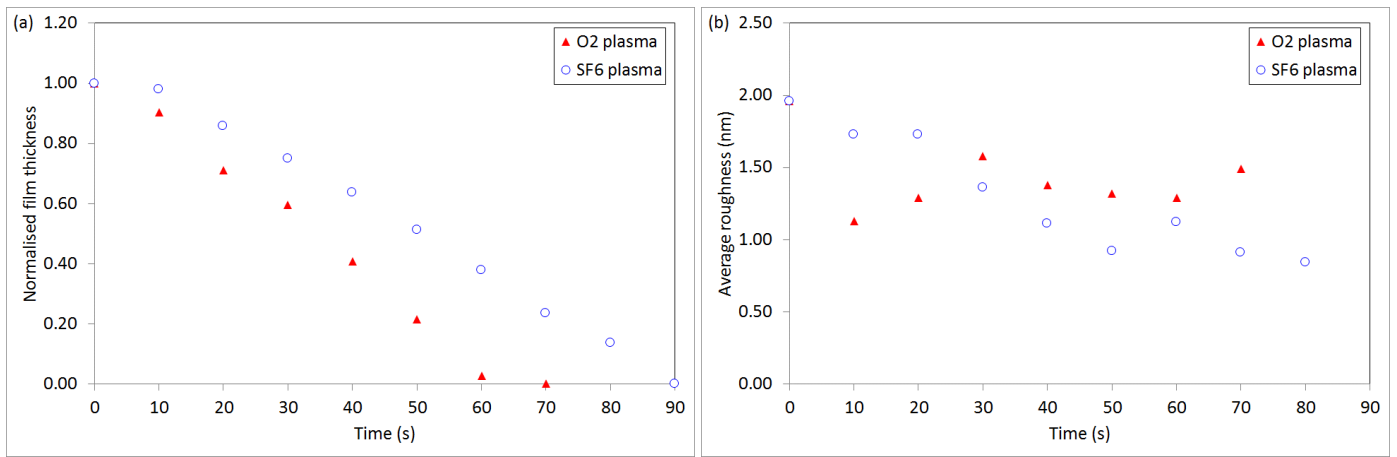


Figure 6. Effect of plasma exposure on  $CF_xO_y$  film thickness and surface roughness.

#### 4. Conclusion

It has been shown that plasma-enhanced chemical vapour deposited fluoropolymer films formed from octafluorocyclobutane is an important material with many industrially relevant applications. By investigating a number of key physical degradation processes, the data presented here suggests that these films have greater potential than has previously been exploited. It has been shown that submicron thick fluoropolymer films can recover from significant scratches. Thinner films where the scratches may have penetrated to the substrate showed a ploughing effect whereby material is pushed aside rather than being plastically compressed or removed as a chip. This phenomena was strongly influenced by film thickness and temperature suggesting polymer mobility and the ability of displaced material to re-bond with the remaining film is a critical factor in the scratch resistivity of a film.

Films were also exposed to a range of environmental conditions experienced during various manufacturing processes including exposure to ultraviolet (UV) radiation of 254 and 365 nm wavelengths in air, nitrogen and under vacuum and exposure to oxygen and sulphur hexafluoride (SF<sub>6</sub>) plasma, the latter being commonly used in conjunction with C<sub>4</sub>F<sub>8</sub> during DRIE processes. Exposure to 365 nm UV in air and 254 nm UV in nitrogen resulted in a minimal loss of material. However, exposure to 254 nm UV in air and under vacuum (reduced air pressure) resulted in significant material loss over 21 h. Similar reactions are observed upon exposure to oxygen plasma, which resulted in a near constant loss rate of material. A similar trend was observed upon exposure to SF<sub>6</sub> plasma, even though the degradation mechanism is different.

Thermo-oxidative studies were conducted through cyclic heating in air. At 100°C, little material loss was noted after 21 hrs, however, at 200°C, 20% mass loss was observed at 21 hrs and 30% mass loss after 63 hrs, suggesting these films have poor thermal stability at 200°C. Given the species generated from the degradation products of C<sub>4</sub>F<sub>8</sub> that form the films are common to several other potential fluorocarbon precursor gases, the results presented here are quite general.

#### Acknowledgments

The JPK Instrument NanoWizard II AFM used in this research was obtained through Birmingham Science City: Innovative Uses for Advanced Materials in the Modern World (West Midlands Centre for Advanced Materials Project 2), with support from Advantage West Midlands (AWM) and part funded by the European Regional Development Fund (ERDF).

#### References

1. Wasilik, M.; Chen, N.; Deep reactive ion etch conditioning recipe, *Proc. Soc. Photo-Opt. Ins.*, **2004**, 5342, 103-110.
2. Li, X.; et al.; Effects of Ar and O<sub>2</sub> additives on SiO<sub>2</sub> etching in C<sub>4</sub>F<sub>8</sub>-based plasmas, *Journal of Vacuum Science & Technology A: Vacuum, Surfaces, and Films*, **2003**, 21(1), 284-93.
3. Kazumi, H.; Hamasaki, R.; Tago, K.; Model prediction of radical composition in plasmas and correlation with measured etch characteristics of silicon dioxide, *Plasma Sources Science and Technology*, **1996**, 5(2), 200.
4. Lärmer, F.; Schlip, A.; A method of anisotropically etching silicon, **1996**, Licensed from Robert Bosch GmbH: US Patent No. 5,501,893.
5. Blauw, M. A.; Zijlstra, T.; Van der Drift, E.; Balancing the etching and passivation in time-multiplexed deep dry etching of silicon, *Journal of Vacuum Science & Technology B: Microelectronics and Nanometer Structures Processing, Measurement, and Phenomena*, **2001**, 19(6), 2930-2934.
6. Tang, Y.; et al.; Ultra deep reactive ion etching of high aspect-ratio and thick silicon using a ramped-parameter process, *Journal of Microelectromechanical Systems*, **2018**, 99, 1-12.
7. Muraka, S. P.; Eizenberg, M.; Sinha, A.K.; eds.; Interlayer dielectrics for semiconductor technologies. Vol. 1. Elsevier, **2003**.
8. Ariel, N.; Eizenberg, M.; Tzou, E.; (1999). The study of fluorinated amorphous carbon as low-k dielectric and its interface with Cu metallization. In *Low-Dielectric Constant Materials and Applications in Microelectronics*, **1999**, 565, 203–208.

9. Kazuhiko, E.; Fluorinated amorphous carbon as a low-dielectric-constant interlayer dielectric, *MRS Bulletin*, **1997**, 22(10), 55-58.
10. Dalvi, V.H.; Rossky, R.J.; Molecular origins of fluorocarbon hydrophobicity, *Proceedings of the National Academy of Sciences*, **2010**, 107(31), 13603-13607.
11. Man, P.F.; Gogoi, B.P.; Mastrangelo, C.H.; Elimination of post-release adhesion in microstructures using conformal fluorocarbon coatings, *Journal of Microelectromechanical systems*, **1997**, 6(1), 25-34.
12. Duksun, H.; Moon S.Y.; Rapid formation of transparent superhydrophobic film on glasses by He/CH<sub>4</sub>/C<sub>4</sub>F<sub>8</sub> plasma deposition at atmospheric pressure, *Plasma Processes and Polymers*, **2015**, 12(2), 172-179.
13. Tsougeni, K.; Papageorgiou, D.; Tserepi, A.; Gogolides, E.; "Smart" polymeric microfluidics fabricated by plasma processing: controlled wetting, capillary filling and hydrophobic valving. *Lab on a Chip*, **2010**, 10(4), 462-469.
14. Han, J.; Flachsbart, B.; Masel, R.I.; Shannon, M.A.; Micro-fabricated membrane gas valves with a non-stiction coating deposited by C<sub>4</sub>F<sub>8</sub>/Ar plasma, *Journal of Micromechanics and Microengineering*, **2008**, 18(9), 095015.
15. Vasudev, M.C.; Anderson, K.D.; Bunning, T.J.; Tsukruk, V.V.; Naik, R.R.; Exploration of plasma-enhanced chemical vapor deposition as a method for thin-film fabrication with biological applications, *ACS applied materials & interfaces*, **2013**, 5(10), 3983-3994.
16. Intranuovo, F.; Favia, P.; Sardella, E.; Ingrosso, C.; Nardulli, M.; d'Agostino, R.; Gristina, R.; Osteoblast-like cell behavior on plasma deposited micro/nanopatterned coatings, *Biomacromolecules*, **2010**, 12(2), 380-387.
17. Labelle, C.B.; Opila, R.; Kornblit, A; Plasma deposition of fluorocarbon thin films from c-C<sub>4</sub>F<sub>8</sub> using pulsed and continuous RF excitation, *Journal of Vacuum Science & Technology A: Vacuum, Surfaces, and Films*, **2005**, 23(1), 190-196.
18. Vasenkov, A.V.; Li, X., Oehrlein, G.S.; Kushner, M.J.; Properties of c-C<sub>4</sub>F<sub>8</sub> inductively coupled plasmas. II. Plasma chemistry and reaction mechanism for modeling of Ar/c-C<sub>4</sub>F<sub>8</sub>/O<sub>2</sub> discharges, *Journal of Vacuum Science & Technology A: Vacuum, Surfaces, and Films*, **2004**, 22(3), 511-530.
19. Milella, A.; Palumbo, F.; Favia, P.; Cicala, G.; d'Agostino, R.; Continuous and Modulated Deposition of Fluorocarbon Films from c-C<sub>4</sub>F<sub>8</sub> Plasmas, *Plasma Processes and Polymers*, **2004**, 1(2), 164-170.
20. Martin, I.T.; Malkov, G.S.; Butoi, C.I.; Fisher, E.R.; Comparison of pulsed and downstream deposition of fluorocarbon materials from C<sub>3</sub>F<sub>8</sub> and c-C<sub>4</sub>F<sub>8</sub> plasmas, *Journal of Vacuum Science & Technology A: Vacuum, Surfaces, and Films*, **2004**, 22(2), 227-235.
21. Cuddy, M.F.; Fisher, E.R.; Contributions of CF and CF<sub>2</sub> Species to Fluorocarbon Film Composition and Properties for C<sub>x</sub>F<sub>y</sub> Plasma-Enhanced Chemical Vapor Deposition, *ACS applied materials & interfaces*, **2012**, 4(3), 1733-1741.
22. Takahashi, K.; Itoh, A.; Nakamura, T.; Tachibana, K.; Radical kinetics for polymer film deposition in fluorocarbon (C<sub>4</sub>F<sub>8</sub>, C<sub>3</sub>F<sub>6</sub> and C<sub>5</sub>F<sub>8</sub>) plasmas, *Thin Solid Films*, **2000**, 374(2), 303-310.
23. Hubert, J.; Vandencastele, N.; Mertens, J.; Viville, P.; Dufour, T.; Barroo, C.; Visart de Bocarmé, T.; Lazzaroni, R.; Reniers, F.; Chemical and physical effects of the carrier gas on the atmospheric pressure PECVD of fluorinated precursors, *Plasma Processes and Polymers*, **2015**, 12(10), 1174-1185.
24. Cheneler, D.; Bowen, J.; Evans, S.D.; Górzny, M.; Adams, M.J.; Ward, M.C.L.; Characteristics and durability of fluoropolymer thin films, *Polymer Degradation and Stability*, **2011**, 96, 561-565.
25. Cheneler, D.; Bowen, J.; Degradation of polymer films, *Soft Matter*, **2013**, 9, 344-358.
26. Brostow, W.; Bujard, B.; Cassidy, P.E.; Hagg, H.E.; Montemartini, P.E.; Effects of fluoropolymer addition to an epoxy on scratch depth and recovery, *Materials Research Innovations*, **2002**, 6(1), 7-12.
27. Bowen, J.; Cheneler, D.; Selecting suitable image dimensions for scanning probe microscopy. *Surfaces and Interfaces*, **2017**, 9, 133-142.
28. Xiang, C.; Sue, H.J.; Chu, J.; Coleman, B.; Scratch behavior and material property relationship in polymers, *Journal of Polymer Science Part B: Polymer Physics*, **2001**, 39(1), 47-59.
29. Cheneler, D.; Mehrban, N.; Bowen J.; Spherical indentation analysis of stress relaxation for thin film viscoelastic materials, *Rheologica Acta*, **2013**, 52(7), 695-706.